ACS APPLIED MATERIALS & INTERFACES

Research Article

www.acsami.org

Interface-Induced Crystalline Ordering and Favorable Morphology for Efficient Annealing-Free Poly(3-hexylthiophene): Fullerene Derivative Solar Cells

Shuyan Shao,[†] Jian Liu,[†,‡] Jidong Zhang,[†] Baohua Zhang,[†] Zhiyuan Xie,*[,†] Yanhou Geng,[†] and Lixiang Wang[†]

[†]State Key Laboratory of Polymer Physics and Chemistry, Changchun Institute of Applied Chemistry, Chinese

[‡]Academy of Sciences, Graduate School of Chinese Academy of Sciences, Changchun 130022, People's Republic of China

Supporting Information

ABSTRACT: A simple approach to fabricate high-efficiency annealing-free poly(3-hexylthiophene): [6,6]-phenyl C_{61}-butyric acid methyl ester (P3HT:PCBM) solar cells is reported by using p-type CuI to substitute PEDOT:PSS as anode buffer layer. It is found that the P3HT:PCBM blend films deposited on CuI surface show different orientation of crystalline P3HT domains and phase separation from those deposited on PEDOT:PSS surface. A nanoscale phase separation of P3HT and PCBM with domain sizes about 10−30 nm is formed for the P3HT:PCBM blend films deposited on CuI surface. Absorption and grazing incidence X-ray diffraction (GIXRD) experiments indicate that the CuI layer not only induces the self-organization of P3HT chains into well-ordered structure but also results in the vertical orientation of $\pi-\pi$ stacking planes of P3HT with respect to the substrate which is favorable for the hole collection in polymer solar cells. Hole-transport investigation discloses that hole mobility of the as-spincast P3HT:PCBM blend film on CuI surface is increased with 3 orders of magnitude compared to the P3HT:PCBM film deposited on PEDOT:PSS. A power conversion efficiency of 3.1% for the as-spincast P3HT:PCBM solar cell with CuI buffer layer is about 4-fold enhancement compared to 0.83% of the control device with PEDOT:PSS, and is comparable to the reported P3HT:PCBM solar cells subjected to post thermal treatments. This work implies that interfacial engineering is a promising approach for manipulating morphology of active layer and can potentially simplify the process and shorten the fabrication time of polymer solar cells in low-cost roll-to-roll manufacturing.

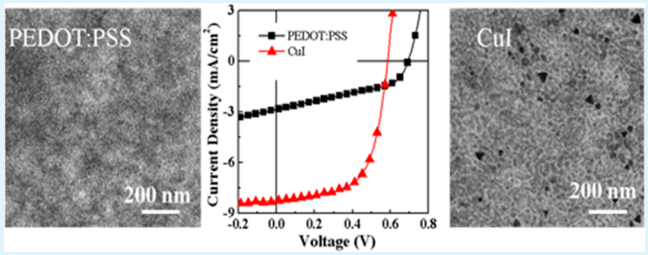

KEYWORDS: *polymer solar cells, bulk heterojunction, chain orientation, morphology, hole transport, interface engineering*

1. INTRODUCTION

Polymer solar cells (PSCs) have been regarded as a promising candidate for renewable energy sources because of their potential advantages of flexible and low-cost fabrication through roll-to-roll processing technology.[1−12] Bulk heterojunction (BHJ), based on blends of electron-donating conjugated polymers and high-electron-affinity fullerene derivatives, has become the most successful device structure for PSCs in order for efficient exciton dissociation due to short exciton diffusion length in conjugated polymers.[13−17] In addition to the efficient exciton dissociation, the collection of photogenerated holes and electrons is another major issue in determining the final photovoltaic performance of the cells. Because of the disordered structure of the blends, the donor and acceptor domains in BHJ active layer are required to form percolated networks with few charge-trapping sites or "dead ends" for realizing the effective transport and collection of separated holes and electrons. Low charge mobility or large mobility difference of holes and electrons in the BHJ active layer would result in sever charge recombination, leading to a low power conversion efficiency (PCE).[18,19] Therefore, the BHJ morphology needs to be well-optimized to trade-off the two issues. As a widely investigated blend of Regioregular poly(3-hexylthiophene) (P3HT) and [6,6]-phenyl C_{61}-butyric acid methyl ester (PCBM), some strategies toward constructing the nanoscale donor and acceptor percolated networks with high hole and electron mobilities have been well developed, including post thermal annealing, solvent-vapor annealing, controlling the solvent evaporation rate, adding high-boiling-point processing additives, etc.[20−27] As a potential low-cost photovoltaic technology, these kinds of approaches would increase the complexity of fabricating the PSCs in large-area roll-to-roll manufacturing.

Water-soluble poly(3,4-ethylenedioxythiophene):poly(styrene sulfonate) (PEDOT:PSS) has been widely used as an anode buffer layer to modify indium−tin oxide (ITO) anode in order for facilitating hole extraction in a typical device structure. However, it was reported that a high content of

Received: August 23, 2012
Accepted: September 18, 2012
Published: October 1, 2012

dx.doi.org/10.1021/am3017653 | ACS Appl. Mater. Interfaces 2012, 4, 5704−5710

insulating species (i.e., PSS) was formed on top surface of the PEDOT:PSS film due to higher surface free energy of PSS than PEDOT, resulting in increased interfacial resistance.[28] Campoy-Quiles et al. modeled the vertical composition profile of P3HT:PCBM blend films on PEDOT:PSS surface by using angle-variable spectroscopic ellipsometry and found a concentration gradient varying from PCBM-rich near PEDOT:PSS side to P3HT-rich adjacent to the free surface, which is not an ideal composition profile for efficient charge collection in regular-configuration PSCs.[29] Moreover, PEDOT:PSS is also concerned with the inherent device instability due to its hygroscopic and hydrophilic nature.[30−32] Research by Norrman et al. showed fast degradation of inverted polymer solar cell in humidity atmosphere.[31] Recent studies by Dupont et al. demonstrated poor adhesion between hydrophobic active layer and hydrophilic PEDOT:PSS layer, which is unfavorable for mechanical stability of the device.[32] Transition metal oxides, such as NiO, MoO_3, and V_2O_5, etc., have been widely used as anode buffer layers in PSCs to replace PEDOT:PSS, and comparable or even higher PCEs have been achieved.[33−36] It has been demonstrated that the crystalline ordering and molecular orientation of P3HT can be tuned by modifying the surface property of underneath substrate.[37−39] However, little work has been done to investigate the effect of surface properties of the anode buffer layer on the crystalline ordering and phase separation of P3HT:PCBM blend and final photovoltaic performance.

CuI is a *p*-type inorganic semiconductor material with a large bandgap of 3.1 eV and can be potentially applied as transparent anode buffer layer in PSCs. Herein, CuI is used to replace PEDOT:PSS as the anode buffer layer to fabricate P3HT:PCBM blend solar cells and its effect on the P3HT:PCBM morphology and the photovoltaic performance of the resulted solar cells is studied in detail. It is found that the CuI buffer layer not only provides an ohmic contact with the active layer, but also causes different orientation of crystalline P3HT domains and nanoscale phase separation of P3HT:PCBM blend as compared to the PEDOT:PSS layer. A nanoscale phase separation of P3HT and PCBM with domain sizes about 10−30 nm is formed for the P3HT:PCBM blend film deposited on CuI surface without thermal or solvent annealing. The CuI layer not only induces the self-organization of P3HT chains into well-ordered structure, but also results in the vertical orientation of $\pi-\pi$ stacking planes of P3HT with respect to the substrate, which is favorable for facilitating hole collection in polymer photovoltaic cells. The hole mobility of the as-spincast P3HT:PCBM blend film deposited on CuI surface is increased with 3 orders of magnitude compared to the as-spincast P3HT:PCBM film deposited on PEDOT:PSS. A PCE of 3.1% for the as-spincast P3HT:PCBM solar cell with CuI buffer layer is about 4-fold enhancement compared to 0.83% of the control device with PEDOT:PSS, and is comparable to the reported P3HT:PCBM solar cells subjected to post treatments. This work implies that interfacial engineering is a promising approach for manipulating morphology of active layer and can potentially simplify the process and shorten the fabrication time of PSCs in low-cost roll-to-roll manufacturing.

2. EXPEIMENTAL SECTION

Materials. P3HT with a weight-average molecular weight (M_w) of 3.0×10^4 (regioregularity >96%) was purchased from Solarmer Energy Co. and PCBM with a purity of 99% was purchased from American Dye Source Co. CuI (purity >99%) was purchased from Sigma-Aldrich Co. All the materials are used as received.

Fabrication and Measurement of PSCs. The ITO-coated glass substrate with a sheet resistance of 10 Ohm/square was cleaned with detergent and deionized water in sequence and then dried at 120 °C for 30 min in an oven. The cleaned ITO substrate was treated with UV-ozone cleaner for 10 min. For the CuI-based PSCs, the CuI buffer layer with different thicknesses was evaporated atop the ITO substrate in vacuum at a base pressure of 7×10^{-4} Pa. For the PEDOT:PSS-based PSCs, a 40-nm-thick PEDOT:PSS (Baytron P4083) layer was spin coated onto the ITO substrate and baked at 120 °C for 30 min in ambient atmosphere. A chlorobenzene solution comprising P3HT (11 mg mL^{-1}) and PCBM (11 mg mL^{-1}) was spin-coated on top of the PEDOT:PSS or CuI layers to produce a 110-nm-thick active layer. Finally, the devices were completed by depositing a bilayer of LiF (1 nm) and Al (100 nm) cathode on top of the active layer in vacuum under base pressure of 4×10^{-4} Pa. The PSCs with solution-processed CuI anode buffer layer was obtained by spin-coating CuI nanoparticle dispersion (0.25 mg/mL) in ethanol on top of the ITO substrate. The illuminated current density−voltage ($J-V$) characteristics of the photovoltaic cells were tested using a Keithley 236 source meter under 100 mW cm^{-2} AM 1.5G simulated solar light. An Oriel 150W solar simulator with an AM 1.5G filter was used to provide an intensity of 100 mW cm^{-2} for illumination of the photovoltaic cells. The light intensity was determined by a calibrated silicon diode with KG-5 visible color filter. The external quantum efficiency (EQE) was measured under short-circuit condition with a lock-in amplifier (SR830, Stanford Research System) at a chopping frequency of 280 Hz during illumination with the monochromatic light from a Xenon lamp.

Thin Film Characterization. Scanning electron microscopy (SEM) observation was conducted on XL 30ESEM-FEG scanning electron microscope operated at an acceleration voltage of 150 kV. Water contact angle test was performed on a DSA10 Control UNIT. Transmission electron microscopy (TEM) of the P3HT:PCBM blend films was performed on JEOL JEM-1011 transmission electron microscope operated at an acceleration voltage of 100 kV. The samples for TEM observation were obtained by stripping the active layer off the underlying PEDOT:PSS layer and then transferred onto a carbon-coated copper grid. UV−vis spectra were recorded on a Perkin-Elmer 35UV−vis spectrophotometer on quartz substrates. The out-of-plane grazing incident X-ray diffraction was measured by using Bruker D8 Discover X-ray diffractometer. The in-plane grazing incident X-ray diffraction were measured at Shanghai Synchrotron Radiation Facility on beamline 14B (λ = 0.124 nm) using Huber diffractometer with scintillation counter and Mar345 detector.

3. RESULTS AND DISCUSSION

An ideal anode buffer layer material should be highly transparent in visible region to ensure efficient solar absorption of the active layer and highly conductive to reduce the series resistance. CuI is a kind of p-type inorganic semiconductor with a band gap of 3.1 eV and has been applied as hole collector in dye-sensitized solar cells (DSSCs) because of its good conductivity and proper energy level.[40−42] For polymer-based solar cells, the work function (WF) of the anode buffer layer should be well matched with the highest occupied molecular

orbital (HOMO) level of the polymer donor in order to facilitate hole collection. Herein, the ITO/CuI interfacial electronic structure is investigated via the ultraviolet photoelectron spectroscopy (UPS) measurement. Three different CuI layers with thicknesses of 1.3, 5.4, and 8.1 nm (i.e., CuI-A, CuI-B, and CuI-C, respectively) were thermally deposited on ITO substrates for the measurement. These kinds of CuI films are highly transparent in visible region (see Figure S1 in the Supporting Information). The UPS spectra of the CuI layers deposited on ITO substrate together with the ITO sample are shown in Figure 1. The WF of ITO is estimated to be −4.5 eV.

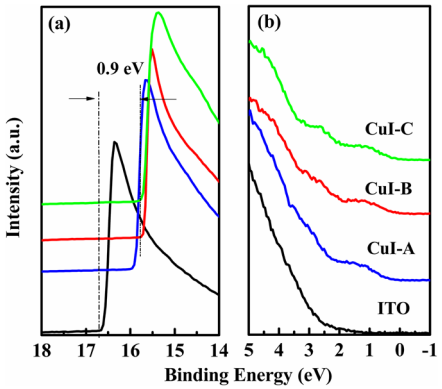

Figure 1. (a) High binding energy and (b) low binding energy panel of UPS spectra of the ITO and different CuI films deposited on top of ITO substrate.

When the CuI films with different thicknesses were deposited onto the ITO surface, the secondary electron cutoff of the CuI films shifts toward lower binding energies about 0.9 eV compared to that of ITO, suggesting a higher WF of CuI. The WF of CuI films is estimated to be about −5.4 eV. The WF of CuI ensures an Ohmic contact between CuI and HOMO of P3HT, and thus facilitates the hole extraction. It is also noticed that the UPS spectra of the three CuI samples have nearly identical shape and position, indicating that 1.3-nm-thick CuI (CuI-A) completely covers the ITO surface.

Scanning electron microscopy (SEM) measurements were carried out to observe the surface morphologies of different CuI films. Figure 2 shows the SEM images of different CuI layers

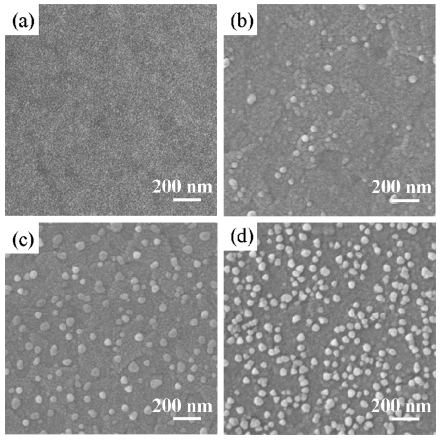

Figure 2. SEM images of different anode buffer layers deposited on ITO substate: (a) PEDOT:PSS (40 nm), (b) CuI-A, (c) CuI-B, and (d) CuI-C.

(CuI-A, CuI-B, and CuI-C) along with the PEDOT deposited on ITO substrate. As shown in Figure 2a, the spincoated PEDOT:PSS film exhibits a very smooth surface. In contrast to spincoated PEDOT:PSS film, the thermally deposited CuI films shows a different morphology. At the initial stage of CuI deposition, the CuI molecules can form a continuous smooth film on the ITO surface. When CuI is further deposited, the discontinuous CuI islands are formed on the smooth CuI films as shown in Figure 2c-d. With the increase of the token thicknesses of CuI, the number of CuI islands increases. The height of these CuI islands is ranged at 20−60 nm estimated by atomic force microscopy (AFM) measurement (see Figure S2 in the Supporting Information). The thicknesses of the underneath continuous CuI layer is determined by fitting the ellipsometry measurement. The thicknesses of the underneath continuous CuI layers were calculated to be 1.3, 5.4, and 8.1 nm for the CuI-A, CuI-B, and CuI-C films, respectively. Water contact angle experiment was carried out on ITO/PEDOT:PSS and ITO/CuI−B substrates to explore the surface properties of PEDOT:PSS and CuI films (see Figure S3 in the Supporting Information). Water contact angles of 93.6 and 49.3° are measured at the CuI-B and PEDOT:PSS surfaces, indicating a highly hydrophobic surface of the CuI films.

Figure 3 shows transmission electron microscopy (TEM) images of P3HT:PCBM blend films deposited on PEDOT:PSS

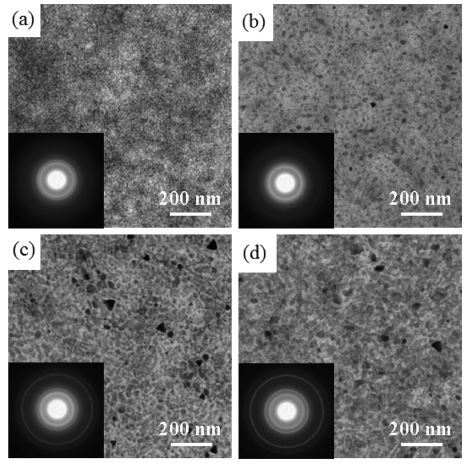

Figure 3. TEM images of the P3HT:PCBM blend films deposited on different anode buffer layer layers: (a) PEDOT:PSS, (b) CuI-A, (c) CuI-B, and (d) CuI-C.

or CuI buffer layers. The light and gray regions in the images were assigned to the P3HT-rich and PCBM-rich domains, respectively. Some dark spots presented in CuI-based P3HT:PCBM films were attributed to residual CuI nanocrystals when the P3HT:PCBM blend layer was stripped off the buffer layer, which was verified by (111) and (220) reflection rings in the selected area electron diffraction (SAED) pattern.[43,44] As shown in Figure 3a, the P3HT:PCBM layer atop PEDOT:PSS layer demonstrates an almost featureless film morphology, indicating intimate mixing of P3HT and PCBM molecules. This kind of morphology would result in poor charge collection and hence poor photovoltaic performance. In contrast, the P3HT:PCBM films deposited atop CuI buffer layers present obvious phase separation of P3HT and PCBM. As shown in Figure 3c, a clear P3HT and PCBM phase separation in P3HT:PCBM film deposited atop the CuI-B buffer layer with domain size of 10−30 nm is formed, which would be favorable

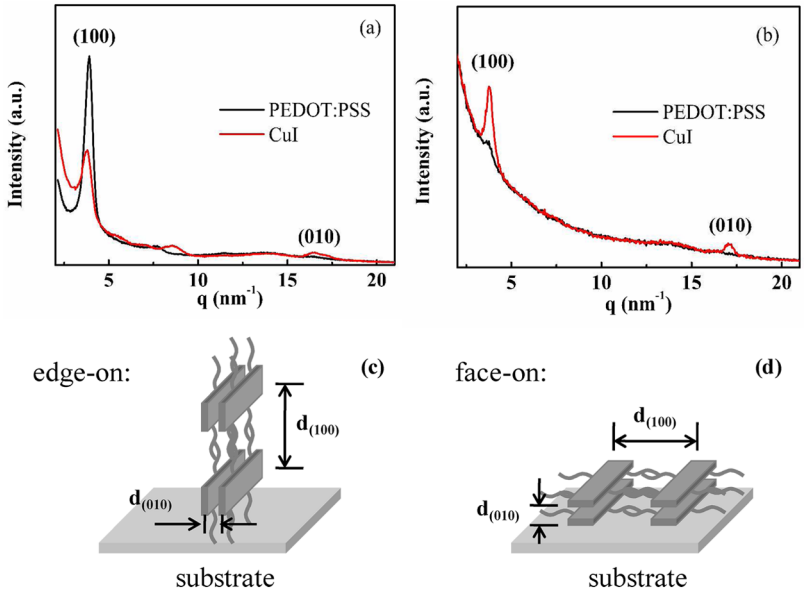

Figure 4. (a) Out-of-plane and (b) in-plane GIXRD patterns of the pristine P3HT:PCBM films spin-coated on PEDOT:PSS or CuI buffer layers. Schematic of edge-on (c) or face-on orientation of P3HT chains with respect to the substrate.

for exciton dissociation and charge collection. Previous studies have shown the surface properties of the substrate have great impact on the crystallization and orientation of the above P3HT film.[37,38] Herein, the chlorobenzene solution of P3HT:PCBM blend was spincoated on different anode buffer layers and the resultant P3HT:PCBM film was not subject to any solvent or thermal treatment. Therefore, the morphology difference of P3HT:PCBM blend atop the PEDOT:PSS and CuI layer can be attributed to different interaction between the buffer layer and the P3HT:PCBM active layer. The absorption of the P3HT:PCBM films on the PEDOT:PSS and CuI buffer layers were also measured (see Figure S4 in the Supporting Information). The P3HT:PCBM films deposited atop the CuI buffer layer show stronger vibronic absorption of P3HT at 559 and 606 nm than that of the P3HT:PCBM film deposited atop the PEDOT:PSS layer, indicating improved P3HT chain packing with CuI as the buffer layer.[27]

To learn more about the effect of interfacial layer on the ordering and orientation of P3HT, we performed grazing incidence X-ray diffraction (GIXRD) for the P3HT:PCBM blend layers deposited atop PEDOT:PSS or CuI−B layers. Figure 4a displays out-of-plane GIXRD pattern of P3HT:PCBM films deposited on PEDOT:PSS and CuI buffer layers. Both the samples show strong (100) plane reflection corresponding to lamellar structure of P3HT, implying edge-on orientation of P3HT chains with hexyl side chains perpendicular to the substrate as depicted in Figure 4c. It is noted in Figure 4a that the P3HT:PCBM film deposited on CuI buffer layer also shows (010) plane reflection in out-of-plane pattern, indicating a face-on orientation of P3HT backbones with $\pi-\pi$ stacking planes perpendicular to the substrate as depicted in Figure 4d. Figure 4b displays in-plane GIXRD pattern of P3HT:PCBM films deposited on PEDOT:PSS and CuI buffer layers. The P3HT:PCBM film deposited on PEDOT:PSS layer shows negligible in-plane (100) reflection, implying that P3HT chains are preferentially oriented with edge-on structure. The absence of (010) reflection demonstrates poor $\pi-\pi$ stacking of P3HT chains in the blend film deposited on PEDOT:PSS layer. It is consistent with the absorption results shown in Figure S4 in the Supporting Information. The sharp in-plane (100) reflection for the blend film deposited on CuI substrate further confirms existence of face-on orientation of P3HT. Both in- and out-of-plane (010) reflections verify that crystalline P3HT domains with edge-on and face-on orientation coexist in P3HT:PCBM blend film deposited on CuI layer. The different P3HT orientation in P3HT:PCBM blend film deposited atop the PEDOT:PSS or CuI surfaces may be attributed to different interactions between P3HT and the underlying surfaces. The repulsive interaction between the π electron clouds of P3HT backbone and unshared electron pairs of hydrophilic surface of PEDOT:PSS allows P3HT to form thermodynamically favorable edge-on orientation. Although the strong coordinated interaction between π electrons of P3HT backbones and atomic orbitals of Cu ions causes P3HT chains to lie down on the surface of CuI layer. These lying-down P3HT chains on the CuI surface may act as nucleus to induce P3HT crystallization with face-on orientation. Thus, both the edge-on orientation and surface-induced face-on orientation of P3HT crystals coexist in the P3HT:PCBM blend film deposited atop the CuI buffer layer.

Because the photogenerated charge carriers are collected along the vertical direction of the active layer via donor and acceptor pathways in PSCs, the crystalline P3HT domains with face-on orientation is favorable for hole transport and collection due to the higher hole mobility of P3HT along $\pi-\pi$ stacking direction than that along the lamellar direction.[45] Herein, the effect of different morphology of P3HT:PCBM blend atop PEDOT:PSS or CuI buffer layers on the hole transport is further investigated via the space charge limited current (SCLC) method. Hole-only devices with structures of ITO/PEDOT:PSS/P3HT:PCBM/MoO_3/Al and ITO/CuI−B/P3HT:PCBM/MoO_3/Al were fabricated with MoO_3 as cathode interfacial layer to suppress electron injection. The dark $J-V$ curves of the hole-only devices with PEDOT:PSS or CuI−B buffer layers at room temperature are shown in Figure 5. The electric field-dependent hole mobilities in P3HT:PCBM blends were calculated through the following equation[19]

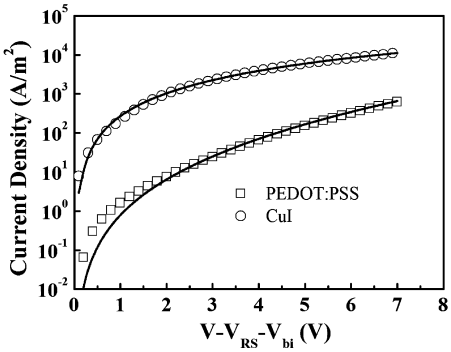

Figure 5. Dark $J-V$ curves of the hole-only devices with a structure of ITO/PEDOT:PSS(40 nm) or CuI–B/P3HT:PCBM (110 nm, as-spincoated)/MoO_3(6 nm)/Al (100 nm) measured at room temperature. Black lines represent the fitting results using a model of single-carrier space-charge-limited current with field-dependent mobility.

$$J = \frac{9}{8}\varepsilon_0\varepsilon_r\mu_h\frac{V^2}{L^3} \quad (1)$$

Where ε_0 is the permittivity of free space, ε_r the relative permittivity of the material, and L the thickness of the active layer. A low room-temperature zero-field hole mobility of 1.0×10^{-7} cm^2 V^{-1} s^{-1} was obtained for the as-spincoated P3HT:PCBM blend deposited on PEDOT:PSS substrates due to amorphous morphology of P3HT and intimate mixing of P3HT and PCBM molecules. The calculated hole mobility is comparable to the value reported by Mihailetchi et al.[19] The reported electron mobility of the pristine P3HT:PCBM blends is estimated to be $2-5 \times 10^{-4}$ cm^2 V^{-1} s^{-1}.[15,23] The difference of 3 orders of magnitude between electron and hole mobilities indicates a strongly unbalanced transport of electrons and holes in the pristine P3HT:PCBM blend films deposited on PEDOT:PSS buffer layer, resulting in severe charge recombination in polymer solar cells.[19,27] The pristine P3HT:PCBM blend film deposited on CuI buffer layer shows a hole mobility of 2.2×10^{-4} cm^2 V^{-1} s^{-1}, 3 orders of magnitude higher than that of the pristine P3HT:PCBM blend film deposited on PEDOT:PSS buffer layer. The dramatic enhancement of hole mobility in the pristine P3HT:PCBM blend film deposited on CuI buffer layer is attributed to presence of crystalline P3HT domains with face-on orientation that improves the hole transport perpendicular to the substrate and a large nanoscale phase separation between P3HT and PCBM induced by the CuI buffer layer. Thus, a more balanced hole and electron transport is realized in the pristine P3HT:PCBM BHJ layer deposited on CuI buffer layer, which is helpful to restrain possible bimolecular charge recombination and improve charge collection.[19]

PSCs with a structure of ITO/CuI-A, CuI–B and CuI–C/P3HT:PCBM (110 nm)/LiF (1 nm)/Al were fabricated to examine the effects of CuI anode buffer layers on photovoltaic performance. A reference cell with a structure of ITO/PEDOT:PSS (40 nm)/P3HT:PCBM (110 nm)/LiF (1 nm)/Al was also fabricated for comparison study. It should be mentioned here that all the devices were fabricated without any pre- or post-thermal treatment after the P3HT:PCBM active layer was spincoated from chlorobenzene solution. The illuminated $J-V$ curves of devices with different anode buffer layers under 100 mW cm^{-2} AM 1.5G simulated solar light are shown in Figure 6a and the photovoltaic parameters of the devices are summarized in Table 1. It can be seen that, the

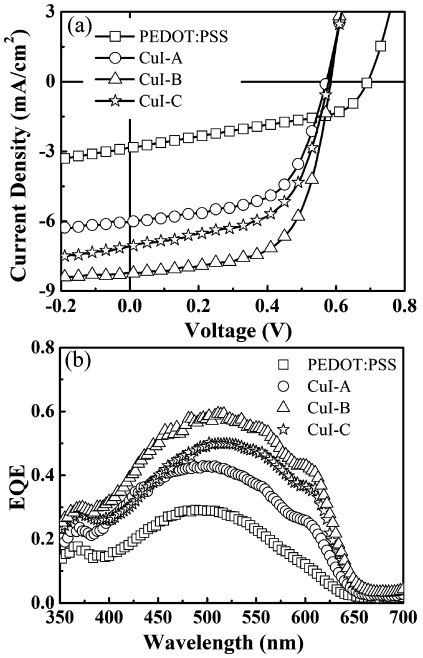

Figure 6. (a) Illuminated $J-V$ characteristics and (b) EQE curves of the P3HT:PCBM (as-spincoated) solar cells with different anode buffer layers.

Table 1. Photovoltaic Parameters of the P3HT:PCBM (as-spincoated) Solar Cells with Different Anode Buffer Layers under AM 1.5G 100 mW cm^{-2} Irradiation

anode buffer layer	V_{OC} (V)	J_{SC} (mA cm^{-2})	FF (%)	PCE (%)
PEDOT:PSS	0.69	2.85	42	0.83
CuI-A	0.57	6.06	59	2.02
CuI–B	0.58	8.21	65	3.10
CuI–C	0.58	7.10	57	2.02

control device with PEDOT:PSS as anode buffer layer demonstrates a short-circuit current (J_{SC}) of 2.85 mA cm^{-2}, an open-circuit voltage (V_{OC}) of 0.69 V, and a fill factor (FF) of 0.42, giving a PCE of 0.83%. The low J_{SC} and FF are mainly attributed to the intimate mixing of P3HT:PCBM blend and low hole mobility of P3HT networks, resulting in a poor charge collection efficiency. On the contrary, the devices with CuI anode buffer layer show considerably improved J_{SC}, FF, and the final PCE. The device with CuI-B buffer layer shows a J_{SC} of 8.21 mA cm^{-2} and a FF of 0.65, and a PCE of 3.1%, respectively, almost a 4-fold increase in PCE compared to that of the device with PEDOT:PSS buffer layer. The considerably enhanced J_{SC} and *FF* are mainly attributed to the favorable nanoscale P3HT:PCBM morphology induced by CuI buffer layer as shown in Figure 3c that improves the exciton dissociation and charge collection. Furthermore, the face-on orientation of P3HT domains on CuI buffer layer may also facilitate hole extraction to the anode and results in a decreased interfacial resistance. It is noted that the PEDOT:PSS-based cell shows a large V_{OC} of 0.69 V, which is commonly presented in the pristine P3HT:PCBM solar cells due to homogeneous morphology of P3HT:PCBM blends.[46] When CuI is used to replace the PEDOT:PSS layer, the V_{OC} of the resulted solar cell is decreased to 0.58 V, comparable to that of the postannealed P3HT:PCBM solar cells. Figure 6b shows the external quantum efficiency (EQE) curves of the photovoltaic cells with

PEDOT:PSS or CuI anode buffer layers. The pristine P3HT:PCBM solar cell exhibits an EQE peak of 30% at a wavelength of 500 nm. When the PEDOT:PSS is replaced by CuI, the EQE of the resultant solar cells is greatly improved. The cell with CuI-B buffer layer shows an EQE peak of 60% at 510 nm with obvious shoulders around 559 and 606 nm attributed to the more ordered structure of P3HT.

We also explored the possibility of preparing the CuI buffer layer with solution-processing technology, which is desirable in large-area roll-to-roll manufacturing. Solution-processable CuI nanoparticles with diameter about 10 nm are easily synthesized following the reference (see Figure S5 in the Supporting Information).[37,38] The P3HT:PCBM blend film deposited atop the solution-processed CuI buffer layer shows strong absorption of P3HT at 559 and 606 nm (see Figure S6 in the Supporting Information), similar to that of the P3HT:PCBM blend film deposited atop the thermally evaporated CuI buffer layer, indicating that the solution-processed CuI can also induce P3HT chain packing and phase separation. The illuminated *J-V* characteristics of the pristine P3HT:PCBM solar cell with solution-processed CuI buffer layer is shown in Figure S7 in the Supporting Information. The PSC with solution-processed CuI buffer layer exhibits a FF of 0.63 and a J_{SC} of 7.65 mA cm^{-2}, comparable to 0.65 and 8.21 mA cm^{-2} of the PSC with thermally deposited CuI buffer layer. However, the V_{OC} drops to 0.54 V, resulting in a PCE of 2.6%. The PCE is about 3-fold higher than that of the device with PEDOT:PSS buffer layer.

4. CONCLUSIONS

In summary, a simple approach to fabricate high-efficiency annealing-free P3HT:PCBM solar cells is reported by using p-type CuI to substitute PEDOT:PSS as anode buffer layer. It is found that the P3HT:PCBM blend films deposited on CuI surface show different orientation of crystalline P3HT domains and phase separation from those deposited on PEDOT:PSS surface. A nanoscale phase separation of P3HT and PCBM with domain sizes about 10−30 nm is formed in the P3HT:PCBM blend films deposited on CuI surface without thermal or solvent annealing. Furthermore, the CuI layer not only induces the self-organization of P3HT chains into well-ordered structure, but also results in the vertical orientation of $\pi-\pi$ stacking planes of P3HT because of strong coordinate interaction between π electrons of P3HT backbones and CuI buffer layer. The hole mobility of the as-spincast P3HT:PCBM blend film on CuI surface are increased with 3 orders of magnitude compared to the as-spincast P3HT:PCBM film deposited on PEDOT:PSS due to the face-on orientation of crystalline P3HT domains and nanoscale P3HT:PCBM morphology induced by CuI. The power conversion efficiency of 3.1% for the as-spincast P3HT:PCBM solar cell with CuI buffer layer is about 4-fold enhancement compared to 0.83% of the control device with PEDOT:PSS, and is comparable to those of reported P3HT:PCBM solar cells subjected to post treatments. This work implies that interfacial engineering is a promising approach for manipulating morphology of active layer and can potentially simplify the process and shorten the fabrication time of polymer solar cells in low-cost roll-to-roll manufacturing.

■ ASSOCIATED CONTENT

Supporting Information

The transmittance spectra of different hole transport layers, atomic force microscopy of evaporated CuI layer, water contact angle of PEDOT:PSS and CuI layers, absorption spectra of P3HT:PCBM blends on top of different hole transport layers, TEM image of solution-processed CuI nanoparticles, absorption spectrum of P3HT:PCBM blends on top of solution processed CuI substrate, the *I−V* curve of the device using solution-processed CuI as hole transport layer. This material is available free of charge via the Internet at http://pubs.acs.org.

■ AUTHOR INFORMATION

Corresponding Author

*Tel.: +86 431 8526 2819. Fax: +86 431 8526 2126. E-mail: xiezy_n@ciac.jl.cn.

Notes

The authors declare no competing financial interest.

■ ACKNOWLEDGMENTS

Z.-Y.X. acknowledges the financial support from the National Natural Science Foundation of China (20921601, 20834005, and 60977026) and 973 Project of Ministry of Science and Technology of China (2009CB623602, 2009CB930603). The authors acknowledge the GIXRD measurement supported by the Shanghai Synchrotron Radiation Facility (SSRF).

■ REFERENCES

(1) Yu, G.; Gao, J.; Hummelen, J. C.; Wudl, F.; Heeger, A. J. *Science* **1995**, *270*, 1789−1791.
(2) Inganäs, O.; Zhang, F. L.; Andersson, M. R. *Acc. Chem. Res.* **2009**, *42*, 1731−1739.
(3) Blom, P. W. M.; Mihailetchi, V. D.; Koster, L. J. A.; Markov, D. E. *Adv. Mater.* **2007**, *19*, 1551−1566.
(4) Dennler, G.; Scharber, M. C.; Brabec, C. J. *Adv. Mater.* **2009**, *21*, 1323−1338.
(5) Cai, W. Z.; Gong, X.; Cao, Y. *Sol. Energy Mater. Sol. Cells* **2010**, *94*, 114−127.
(6) Krebs, F. C. *Sol. Energy Mater. Sol. Cells* **2009**, *93*, 394−412.
(7) Liang, Y. Y.; Xu, Z.; Xia, J. B.; Tsai, S.-T.; Wu, Y.; Li, G.; Ray, C.; Yu, L. P. *Adv. Mater.* **2010**, *22*, E135−E138.
(8) Qin, R. P.; Li, W. W.; Li, C. H.; Du, C.; Veit, C.; Schleiermacher, H. F.; Andersson, M.; Bo, Z. S.; Liu, Z. P.; Inganäs, O.; Wuerfel, U.; Zhang, F. L. *J. Am. Chem. Soc.* **2009**, *131*, 14612−14613.
(9) Søndergaard, R; Hösel, M; Angmo, D; Larsen-Olsen, T. T.; Krebs, F. C. *Mater. Today* **2012**, *15*, 36−49.
(10) Amb, C. M.; Craig, M. R.; Koldemir, U.; Subbiah, J.; Choudhury, K. R.; Gevorgyan, S. A.; Jørgensen, M.; Krebs, F. C.; So, F.; Reynolds, J. R. *ACS Appl. Mater. Interfaces* **2012**, *4*, 1847−1853.
(11) Krebs, F. C.; Fyenbo, J.; Tanenbaum, D. M.; Gevorgyan, S. A.; Andriessen, R.; Remoortere, B.; Galagan, Y.; Jørgensen, M. *Energy Environ. Sci.* **2011**, *4*, 4116−4123.
(12) Krebs, F. C.; Nielsen, T. D.; Fyenbo, J.; Wadstrøm, M.; Pedersen, M. S. *Energy Environ. Sci.* **2010**, *3*, 512−525.
(13) Chu, T.-Y.; Lu, J. P.; Beaupré, S.; Zhang, Y. G.; Pouliot, J.-R.; Wakim, S.; Leclerc, M.; Li, Z.; Ding, J. F.; Tao, Y. *J. Am. Chem. Soc.* **2011**, *133*, 4250−4253.
(14) Seo, J. H.; Gutacker, A.; Sun, Y. M.; Wu, H. B.; Huang, F.; Cao, Y.; Scherf, U.; Heeger, A. J.; Bazan, G. C. *J. Am. Chem. Soc.* **2011**, *133*, 8416−8419.
(15) Huang, F.; Chen, K. S.; Yip, H. L.; Hau, S. K.; Acton, O.; Zhang, Y.; Luo, J. D.; Jen, A. K. Y. *J. Am. Chem. Soc.* **2009**, *131*, 13886−13887.
(16) Woo, C. H.; Beaujuge, P. M.; Lee, O. P.; Fréchet, J. M. J. *J. Am. Chem. Soc.* **2010**, *132*, 15547−15549.

(17) Chang, C. Y.; Wu, C. E.; Chen, S. Y.; Cui, Y. J.; Cheng, C. S.; Wang, Y. L.; Li, Y. F. *Angew. Chem.Int. Ed.* **2011**, *123*, 9558−9562.
(18) Mihailetchi, V. D.; Wildeman, J.; Blom, P.W. M. *Phys. Rev. Lett.* **2005**, *94*, 126602−126606.
(19) Mihailetchi, V. D.; Xie, H. X.; Boer, B.; de, A.; Koster, L. J.; Blom, P. W. M. *Adv. Funct. Mater.* **2006**, *16*, 699−708.
(20) Wang, W. L.; Wu, H. B.; Yang, C. Y.; Luo, C.; Zhang, Y.; Chen, J. W.; Cao, Y. *Appl. Phys. Lett.* **2007**, *90*, 183512−1−3.
(21) Savenije, T. J.; Kroeze, J. E.; Yang, X.; Loos, J. *Adv. Funct. Mater.* **2005**, *15*, 1260−1266.
(22) Padinger, F.; Rittberger, R. S.; Sariciftci, N. S. *Adv. Funct. Mater.* **2003**, *13*, 85−88.
(23) Nguyen, L. H.; Hoppe, H.; Erb, T.; Günes, S.; Gobsch, G.; Sariciftci, N. S. *Adv. Funct.Mater.* **2007**, *17*, 1071−1078.
(24) Li, G.; Yao, Y.; Yang, H.; Shrotriya, V.; Yang, G.; Yang, Y. *Adv. Funct. Mater.* **2007**, *17*, 1636−1644.
(25) Li, G.; Shrotriya, V.; Huang, J.; Yao, Y.; Moriarty, T.; Emery, K.; Yang, Y. *Nat. Mater.* **2005**, *4*, 864−868.
(26) Zhao, Y.; Xie, Z. Y.; Qu, Y.; Geng, Y. H.; Wang, L. X. *Appl. Phys. Lett.* **2007**, *90*, 043504−1−3.
(27) Liu, J. G.; Shao, S. Y.; Wang, H. F.; Zhao, K.; Xue, L. J.; Gao, X.; Xie, Z. Y.; Han, Y. C. *Org. Electron.* **2010**, *11*, 775−783.
(28) Lee, T. W.; Chung, Y.; Kwon, O.; Park, J. J. *Adv. Funct. Mater.* **2007**, *17*, 390−396.
(29) Campoy-Quiles, M.; Ferenczi, T.; Agostinelli, T.; Etchegoin, P. G.; Kim, Y.; Anthopoulos, T. D.; Stavrinou, P. N.; Bradley, D. C.; Nelson, J. *Nat. Mater.* **2008**, *7*, 158−164.
(30) Meyer, J.; Khalandovsky, R.; Görrn, P.; Kahn, A. *Adv. Mater.* **2011**, *23*, 70−73.
(31) Dupont, S. R.; Oliver, M.; Krebs, F. C.; Dauskardt, R. H. *Sol. Energy Mater. Sol. Cells* **2012**, *97*, 171−175.
(32) Norrman, K.; Madsen, M. V.; Gevorgyan, S. A.; Krebs, F. C. *J. Am. Chem. Soc.* **2010**, *132*, 16883−16892.
(33) Liu, F. M.; Shao, S. Y.; Guo, X. Y.; Zhao, Y.; Xie, Z. Y. *Sol. Energy Mater. Sol. Cells* **2010**, *94*, 842−845.
(34) Irwin, M. D.; Buchholz, D. B.; Hains, A. W.; Chang, R. P. H.; Marks, T. J. *Proc. Natl. Acad. Sci.* **2008**, *105*, 2783−2787.
(35) Shrotriya, V.; Li, G.; Yao, Y.; Chu, C.-W.; Yang, Y. *Appl. Phys. Lett.* **2006**, *88*, 073508−1−3.
(36) Manceau, M.; Bundgaard, E.; Carle, J. E. O.; Hagemann, M.; Helgesen, R.; Jørgensen, M.; Krebs, F. C. *J. Mater. Chem.* **2011**, *21*, 4132−4141.
(37) Kim, D. H.; Jang, Y.; Park, Y. D.; Cho, K. *Macromolecules* **2006**, *39*, 5843−5847.
(38) Kim, D. H.; Park, Y. D.; Jang, Y.; Yang, H.; Kim, Y. H.; Han, J. I.; Moon, S.; Park, D. G.; Chang, T.; Joo, M.; Ryu, C. Y.; Cho, K. *Adv. Funct. Mater.* **2005**, *15*, 77−82.
(39) Kline, R. J.; Mcgehee, M. D.; Toney, M. F. *Nat. Mater.* **2006**, *5*, 222−228.
(40) Chen, L. H.; Xue, B. F.; Liu, X. Z.; Li, K. X.; Luo, Y. H.; Meng, Q. B.; Wang, R. L.; Chin, L. Q. *Chin. Phys. Lett.* **2007**, *24*, 555−560.
(41) Perera, V. P. S.; Tennakone, K. *Sol. Energy Mater. Sol. Cells* **2003**, *79*, 249−252.
(42) Rusop, M.; Shirata, T.; Sirimanne, P. M.; Soga, T.; Jimbo, T.; Umeno, M. *Appl. Surf. Sci.* **2006**, *252*, 7389−7394.
(43) Yang, Y.; Liu, S.; Kimura, K. *Chem. Lett.* **2005**, *34*, 902−906.
(44) Yang, Y.; Liu, S.; Kimura, K. *Chem. Lett.* **2005**, *34*, 1158−1167.
(45) Sirringhaus, H.; Brown, P. J.; Friend, R. H.; Nielsen, M. M.; Bechgaard, K.; Langeveld-Voss, B. M. W.; Spiering, A. J. H.; Janssen, R. A. J.; Meijer, E. W.; Herwig, P.; Leeuws, D. M. *Nature* **1999**, *401*, 685−688.
(46) Vandewal, K.; Gadisa, A.; Oosterbaan, W. D.; Bertho, S.; banishoeib, F.; Severen, I. V.; Lutsen, L.; Cleij, T. J.; Vanderzande, D.; Manca, J. V. *Adv. Funct. Mater.* **2008**, *18*, 2064−2070.